J. Anat. (1999) **194**, pp. 89–100 with 10 figures Printed in the United Kingdom

Three dimensional analysis of microaneurysms in the human diabetic retina

J. MOORE[1,2], S. BAGLEY[2], G. IRELAND[2], D. MCLEOD[1] AND M. E. BOULTON[1,2]

[1] *Department of Ophthalmology and* [2] *School of Biological Sciences, University of Manchester, UK*

(*Accepted 6 October 1998*)

ABSTRACT

The retinal vasculature of postmortem normal human and diabetic eyes was studied using an immunohistochemical technique in conjunction with confocal laser scanning microscopy. The technique, which stained for von Willebrand factor, allowed both large areas of the retinal vasculature to be visualised and abnormalities to be studied in detail without disturbing the tissue architecture. Only one microaneurysm, defined as any focal capillary dilation, was observed in 10 normal eyes but numerous microaneurysms were seen in 4 out of 5 diabetic retinas; counts varied between 0 and 26 per 0.41 mm^2 sample area. Microaneurysms were classified into 3 categories according to morphology: saccular, fusiform and focal bulges. Most were saccular, these having no preferred orientation. The majority of microaneurysms were associated with just 2 vessels suggesting they were unlikely to develop at vascular junctions. The majority were observed to originate from the inner nuclear layer and were therefore in the deeper part of the inner retinal capillary plexus. Variation in the staining of microaneurysms may correlate with endothelial dysfunction seen clinically as dye leakage during fluorescein angiography.

Key words: Confocal microscopy; retinal vasculature; diabetic retinopathy.

INTRODUCTION

Microaneurysms are dilations of capillaries which often appear as gross outpouchings of the vessel wall. Although microaneurysms can be found in a variety of vascular beds (e.g. kidney, heart), they are most common in the retinal capillaries of the diabetic eye where they occur chiefly, but not exclusively, on the venous side of the capillary bed (Ashton, 1951, 1963). Large microaneurysms are the first ophthalmoscopic feature to appear in diabetic retinopathy; smaller aneurysms and the associated dye leakage indicative of breakdown of the blood–retinal barrier can be seen with fluorescein angiography. Microaneurysms are often found in close association with focal areas of capillary nonperfusion, as demonstrated by trypsin digests of the retina or fluorescein angiography (Ashton, 1951; Kohner & Dollery, 1970). Unfortunately, the removal of the extravascular tissues by trypsin digestion precludes deriving information about the spatial organisation of microaneurysms within the neural retina. The 3-dimensional (3D) structure of the microvasculature was maintained by Fryczkowski et al. (1991) who produced a vascular cast from one diabetic eye and demonstrated the variability in morphology of diabetic microaneurysms; however removal of extravascular tissue was still required using this technique. Thus we have limited knowledge of the relative frequency of the various types of microaneurysms and their location and orientation within the retina. Previously we have used confocal microscopy together with immunofluorescent staining for von Willebrand factor, an endothelial cell marker, to examine the retinal vasculature of normal eyes (Foreman et al. 1996). The aim of this study was to use the same technique to allow 3D visualisation of retinal capillary microaneurysms in the intact human diabetic retina. Information from 4 retinas was obtained concerning microaneurysm number and distribution, their precise origin and location within the layers of the neuroretina, their size, shape and orientation and the number of vessels associated with each microaneurysm.

Correspondence to Dr M. E. Boulton, University Department of Ophthalmology, Manchester Royal Eye Hospital, Oxford Road, Manchester, M13 9WH, UK. Tel: 0161–275–5249; fax: 0161–276–6354; email: mboulton@man.ac.uk

MATERIALS AND METHODS

Preparation of tissue

Five postmortem eyes from 5 diabetic donors (insulin-treated) (Table 1) and 10 eyes from 10 age-matched donors, who had not been identified as diabetic, were obtained from the National Disease Research Interchange (Philadelphia) and the Manchester Royal Eye Hospital eye bank and examined. The donors were aged between 73 and 81 y. Tissue had been fixed within 24 h postmortem with 10% neutral buffered formalin and, after removal of the anterior segment and the majority of the vitreous, proliferative diabetic retinopathy was excluded by macroscopic examination. The retinas were then dissected from the remaining ocular tissue by a rectangular incision around an area of retina approximately 25 mm × 12 mm including the optic nerve head and macula, main temporal vascular arcades and temporal periphery, followed by gentle detachment from the retinal pigment epithelium using blunt-ended forceps. Any remaining vitreous was carefully cut away and the dissected retinas were washed with phosphate buffered saline (PBS), incubated with 1% α-chymotrypsin (type II, from bovine pancreas, Sigma) in Tris buffered saline (TBS) at 37 °C for 30 min (to help expose epitopes) and permeablised by immersion in 0.2% Triton X-100 in PBS for 1 h.

Immunofluorescent staining

The retinas were stained for von Willebrand factor (vWf), an adhesion factor synthesised in endothelial cells. After blocking against nonspecific binding for 1 h by immersion in 20% normal goat serum in PBS, they were incubated overnight at room temperature with a 1:50 dilution of rabbit antihuman vWf (Dako) in PBS containing 2% normal goat serum. Following a 3 h wash in PBS, retinas were incubated overnight at room temperature with a 1:50 dilution of goat antirabbit fluorescein isothiocyanate (FITC) (Sigma) in PBS containing 2% normal goat serum. After a 3 h wash in PBS, the retinas were flat-mounted vitreous side up in Gelvatol (Rodriquez & Deinhardt, 1960) under glass cover-slips.

Confocal microscopy

Immunostained retinas were examined from the vitreous surface with a Biorad MRC 600 confocal laser scanning attachment mounted on a suitably modified photomicroscope II (Zeiss) using an argon laser (25 mW, Ion Laser Technology) with a BHS filter block (excitation 488 nm). This allowed detection of FITC-labelled vWf associated with the vascular endothelium. The confocal microscope was utilised in different modes described in detail below. Briefly, when higher magnification/high numerical aperture (NA) objectives were used, the instrument was operated in a confocal mode with small pinholes and sharp fluorescence images, free from out of focus blur (Shotton & White, 1989), were collected representing optical sections within the retina. When a very low power objective (× 5) was used with wide pinholes, the microscope was operated in a nonconfocal mode. In all cases captured images were stored on optical disks using an optical drive (Panasonic 7030E).

Vascular maps

In order to visualise the overall topography of the retinal vessels and facilitate location of particular regions of the tissue a series of overlapping images of very low power (× 5 objective, GS, flat lens, NA = 0.18) were captured with the confocal aperture fully open. These images were printed and assembled manually to produce a montage or 'map' of the vasculature of each retina including the optic nerve head, macular and nonmacular temporal regions.

Low power analysis

Random numbers were used as coordinates for positioning the specimen beneath the objective lens. Sample areas 792 × 528 μm in size were imaged with a × 16 objective (Zeiss, plan-neofluor lens, oil immersion, NA = 0.5) so that microaneurysm counts could be made. For each sample area, 10–20 images typically separated by 5 μm were captured (using a Kalman average of 5 and a minimum confocal aperture) through the depth (z) of the retina. Each image was in the retinal (xy)-plane at a different point along the z axis but together formed a z series of images containing 3D information. The region sampled was identified as being within either the macula (defined as a circular area of diameter 5.5 mm with the foveal avascular zone at its centre) or the nonmacular temporal region by identifying the position of the faded area using lower magnification. From each z series the number of microaneurysms, defined in this study as any focal vessel dilation, was counted. Their widths (the distance between their outer borders measured perpendicular to the associated vessel direction) were measured from the appropriate image of z series using the 'length' command in the Comos confocal operating system (Biorad).

High power analysis

Individual images of microaneurysms were also collected at a higher magnification to allow more detailed study. A number of microaneurysms were randomly selected and imaged using the $\times 60$ objective (Nikon, plan-apo lens, oil immersion, NA = 1.4). For each microaneurysm a z series of between 15 and 55 images typically separated by 1.5 μm was produced using a Kalman average of 5 and a minimum confocal aperture. Several images were also collected using an xz scan derived from 512 line scans in the x-axis, each separated by a step in the z-axis of 0.5 μm. This produced images in the xz-plane (xz images) which were used to allow identification of individual retinal layers (made possible by the lack of background staining of nuclei) and the position of the stained microaneurysm within them.

From the z series, the microaneurysms were classified according to (1) origin within the layers of the neuroretina, (2) shape, (3) orientation and (4) number of vessels associated with each microaneurysm. The distance of microaneurysm origin from the vitreoretinal interface (VRI) was measured in layers. Each of the normal retinal layers (nerve fibre/ganglion cell (NFL/GCL), inner plexiform (IPL), inner nuclear (INL), outer plexiform (OPL) and outer nuclear (ONL)) as well as the interface between these layers were counted, the NFL/GCL and ONL being layers 1 and 9 respectively. The layer or interface of microaneurysm origin was defined as the point midway between those associated capillaries that were furthest apart in the z axis.

Microaneurysms were categorised as being (*a*) 'saccular' if the dilation was asymmetric around the long axis of the associated vessel(s), (*b*) 'fusiform' if the dilation was symmetric around the long axis of the associated vessel(s) or (*c*) a 'focal bulge' if too small and irregularly shaped to be classified as (*a*) or (*b*).

If the size of a saccular lesion measured in the z-axis was unevenly distributed at either side of its origin, it was described as having either a choroid or vitreous orientation. If the size of a saccular lesion measured in the xy-plane was unevenly distributed at either side of its origin, it was described as having a lateral orientation.

From the xz images, measurements of maximum microaneurysm size measured as 'z extent' (the distance between outer borders measured in the z axis) were taken using the 'length' command in Comos confocal operating system (Biorad).

Maximum projection images, produced using Confocal Assistant software (Todd Clark Brelje), allowed a presentation of the z series representing composite features throughout the thickness of the retina in that region.

Statistical analysis

All data were tested for normality before statistical analysis and the appropriate parametric or non-parametric tests assigned. Probabilities and percentages were rounded to 2 significant figures. Values of $P < 0.01$ and $P < 0.05$ were considered highly significant and significant respectively and the null hypothesis rejected. All statistical tests were performed using Simfit software (Bardsley, 1993). Average microaneurysm counts were compared between retinas using the Kruskal–Wallis test. Tests for random (Poisson) distribution were performed on count data using the Kolmogorov–Smirnov 1 sample test. Comparisons of average microaneurysm width between retinas were made using the Kruskal–Wallis test and correlations between counts and width determined by calculating Kendall's rank correlation coefficient. Probabilities of a microaneurysm originating in a particular retinal layer were calculated using binomial statistics on the proportion data

$$\frac{\text{number originating in layer 'x'}}{\text{total number.}}$$

Comparisons of the average z extents between groups of microaneurysms classified according to shape were made using the Kruskal–Wallis test. Differences between saccular microaneurysm orientation were analysed by a χ^2 test on a contingency table of counts for the retinas. Correlations between microaneurysm z extent, distance of microaneurysm origin from the vitreoretinal interface and number of associated vessels were determined by calculating Kendall's rank correlation coefficient.

RESULTS

In our illustrations and terminology we have adopted the convention that the retina is oriented vitreous surface up and photoreceptors down, with the 'inner' surface referring to that towards the vitreous and the 'outer' surface referring to that towards the choroid. Specimens were examined from the vitreous surface and 3D information was acquired, by confocal microscopy, as a series of images in the retinal (xy)-plane. These images were taken at different depths within the retina, along the z-axis, and formed a z series. Alternatively, single images in the xz-plane were obtained (termed xz images). Two different terminologies have been used when referring to

Table 1. *Details of diabetic donors*

	Retina I	Retina II	Retina III	Retina IV	Retina V
Donor age (y)	76	79	74	81	73
Donor sex	Female	Male	Male	Female	Male
Duration of diabetes (y)	18	25	25	20	9
Cause of death	Breast cancer	Pulmonary emboli	Myocardial infarction	Cerebrovascular accident	Myocardial infarction

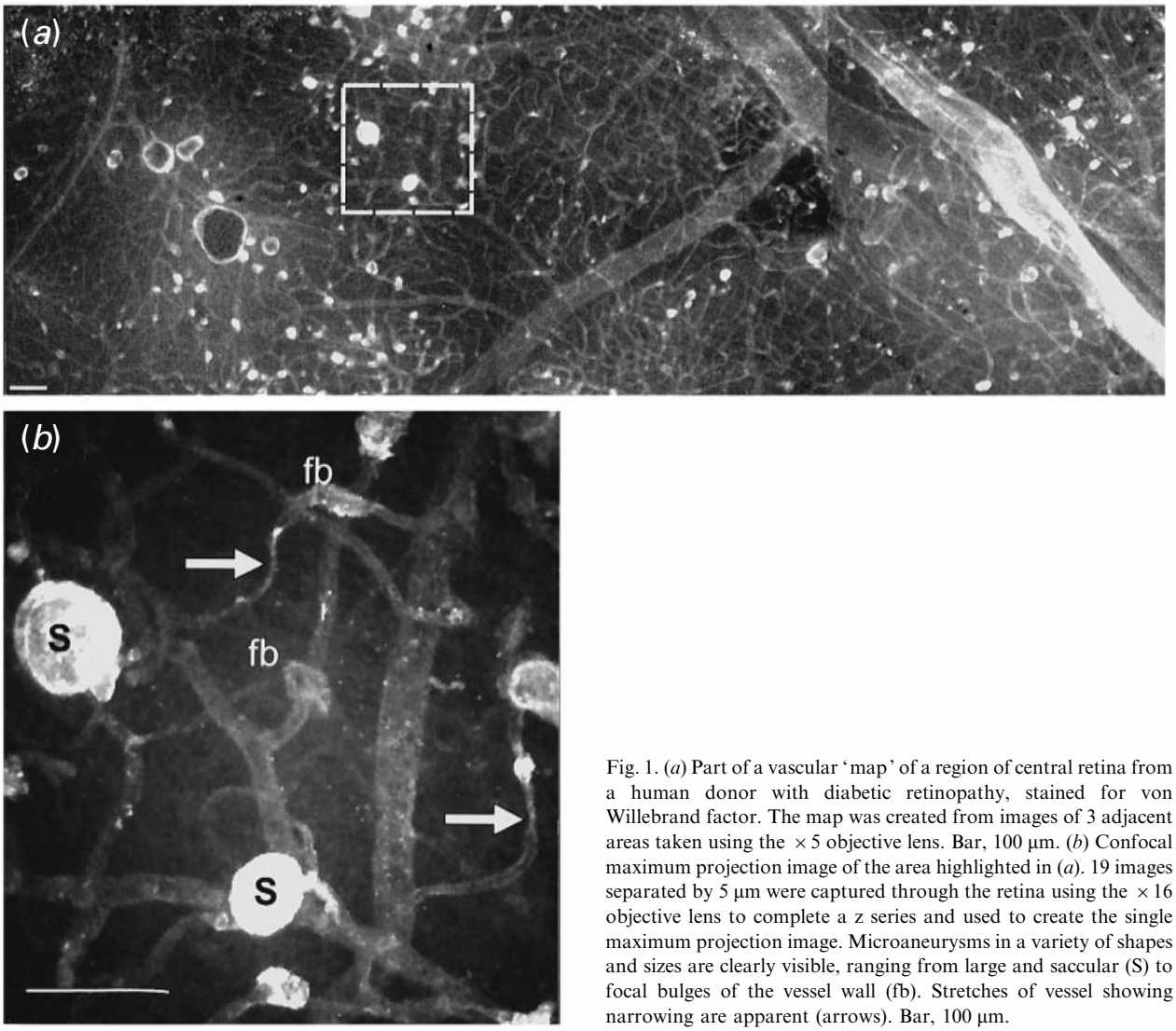

Fig. 1. (*a*) Part of a vascular 'map' of a region of central retina from a human donor with diabetic retinopathy, stained for von Willebrand factor. The map was created from images of 3 adjacent areas taken using the × 5 objective lens. Bar, 100 μm. (*b*) Confocal maximum projection image of the area highlighted in (*a*). 19 images separated by 5 μm were captured through the retina using the × 16 objective lens to complete a z series and used to create the single maximum projection image. Microaneurysms in a variety of shapes and sizes are clearly visible, ranging from large and saccular (S) to focal bulges of the vessel wall (fb). Stretches of vessel showing narrowing are apparent (arrows). Bar, 100 μm.

microaneurysm dimensions depending on which plane the measurement was taken in, width and z extent referring to xy and xz planes respectively. When very low power objectives were used, a single digital image was collected from each field of view and pieced together to produce a 'map' of the tissue.

From the 5 diabetic retinas (Table 1) stained for vWF and examined at very low power, vascular maps (Fig. 1) were produced of the macula and nonmacular temporal regions. They illustrated both large and small vessel networks and delineated the foveal avascular zone. Microaneurysms of a variety of shapes and sizes were clearly visible, ranging from large saccular swellings to focal bulges of the vessel wall (Fig. 1*b*). One of the 5 maps showed no microaneurysms (even at high magnification), and was therefore not used in the subsequent analysis. In the 10 nondiabetic controls examined, only 1 microaneurysm was observed within an otherwise normal-appearing capillary bed.

Table 2. *Number of microaneurysms found in each 792 × 528 μm area sampled randomly*

	Retina I	Retina II	Retina III	Retina IV
Counts	0, 0, 0, 0, 0, 0, 0, 0, 0, 0, 0, 0, 0, 0, 0, 0, 0, 0, 0, 0, 0, 0, 0, 0, 0, 0, 0, 0, 0, 0, 0, 0, 0, 0, 0, 1, 1, 1, 1, 1, 2, 2, 2, 3, 3, 4, 6, 6,	5, 6, 7, 11, 11, 12, 13, 26	2, 2, 4, 5, 6, 6, 7, 8	0, 0, 0, 0, 0, 0, 0, 0, 0, 0, 0, 0, 0, 0, 0, 0, 0, 0, 0, 0, 0, 0, 0, 0, 0, 0, 0, 0, 0, 0, 0, 0, 0, 0, 0, 1, 1, 1, 1, 2, 2, 3, 3, 4
λ* (2dp)	0.75 ± 1.73	11.38 ± 6.75	5 ± 4.47	0.49 ± 1.39
P**	0.014	0.61	1.0	0.41

* λ, Poisson parameter defined here as the average number of lesions per sample area. Variance in the Poisson parameter is estimated using $\lambda \pm 2\sqrt{\lambda}$ which approximates to the 95% confidence limits for a Poisson distribution.
** P, probability of data arising from a Poisson distribution.

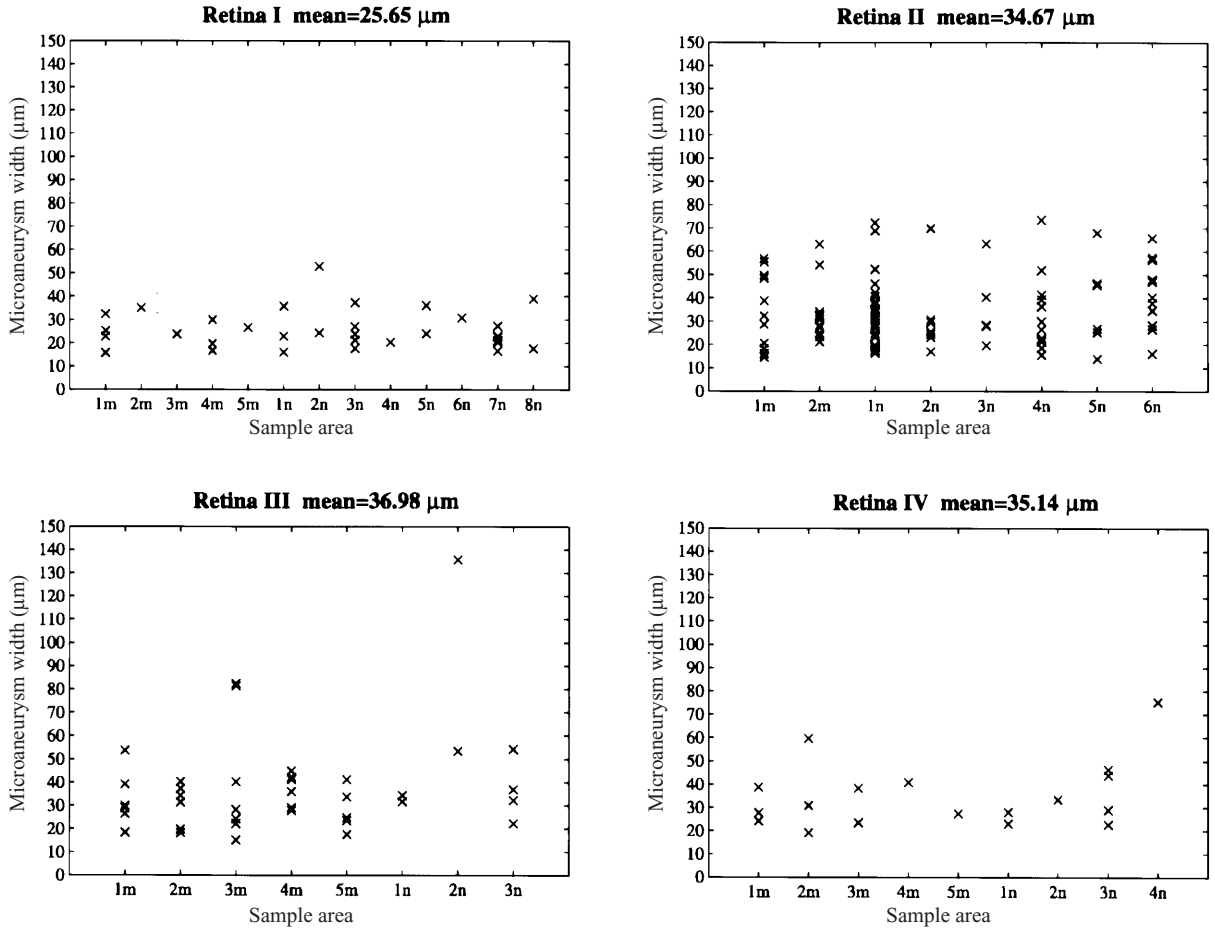

Fig. 2. Microaneurysm widths showing partitioning for sample area. Numbers allocated to sample areas are arbitrary, 'm' and 'n' distinguish sample areas within the macular and nonmacular regions respectively. The width of each microaneurysm within every sample area is illustrated as a data point. The mean quoted for each retina was calculated from widths grouped from all sample areas in that retina and rounded to 2 decimal places.

Low power analysis

Microaneurysm counts within the mapped regions were made from low power analysis of 97 random sample areas (792 × 528 μm) (Table 2). These counts varied between 0 and 26 microaneurysms per sample area. Variation in microaneurysm number was seen between retinas, i.e. the average count per sample area showed significant differences between retinas (comparisons between I and II, I and III, II and IV, III and IV gave $P < 0.0001$, and between II and III gave $P = 0.015$) apart from retinas I and IV ($P = 0.55$). The data were tested for possible fitting to a Poisson distribution indicating random occurrence of microaneurysms. In 3 out of the 4 retinas a random microaneurysm distribution in the retinal plane (xy) was indicated ($P = 0.61$, 1.0 and 0.41 for retinas II, III and IV respectively).

Table 3. *Number of microaneurysms by shape category**

	Retina I	Retina II	Retina III	Retina IV	Totals
Saccular	7 (37%)	17 (85%)	12 (57%)	6 (50%)	42 (58%)
Fusiform	0	0	4 (19%)	3 (25%)	7 (9.7%)
Focal bulge	12 (63%)	3 (15%)	5 (24%)	3 (25%)	23 (32%)

* Analysed following random sampling of 4 retinas at high power.

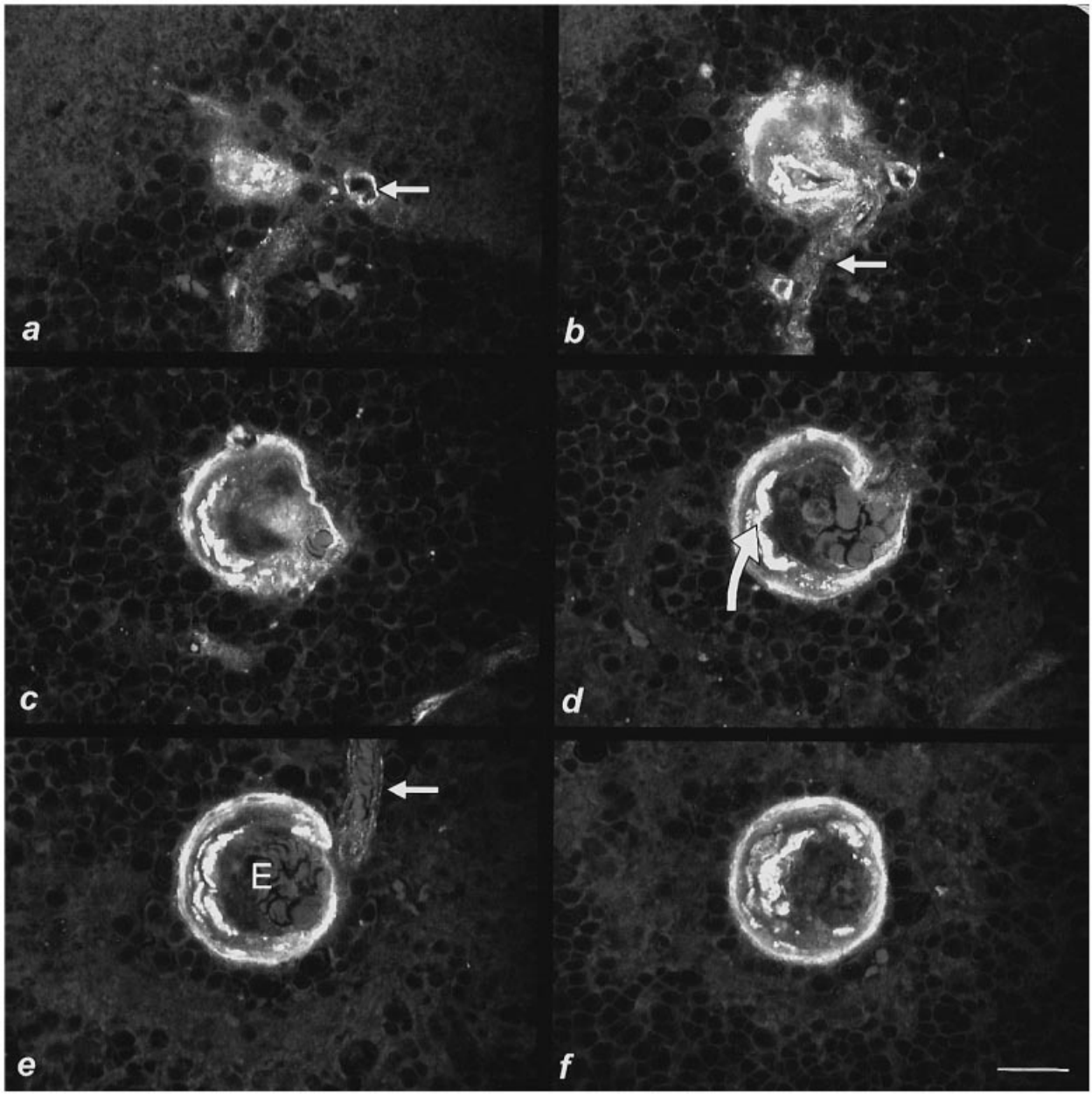

Fig. 3. Montage of images from a confocal z series captured through a saccular microaneurysm stained for von Willebrand factor; each optical section is separated by 4.5 μm. Images were captured, using the ×60 objective lens, from the inner edge of the microaneurysm (*a*) to the outer edge of the micoaneurysm (*f*). Staining of the microaneurysm wall appears much more intense than that of its associated vessels (small arrows) and layers of intense staining are prominent at one side (large curved arrow). The microaneurysm is packed with erythrocytes (E). Nuclei of the surrounding extravascular tissue are visible by virtue of being unstained. Bar, 25 μm.

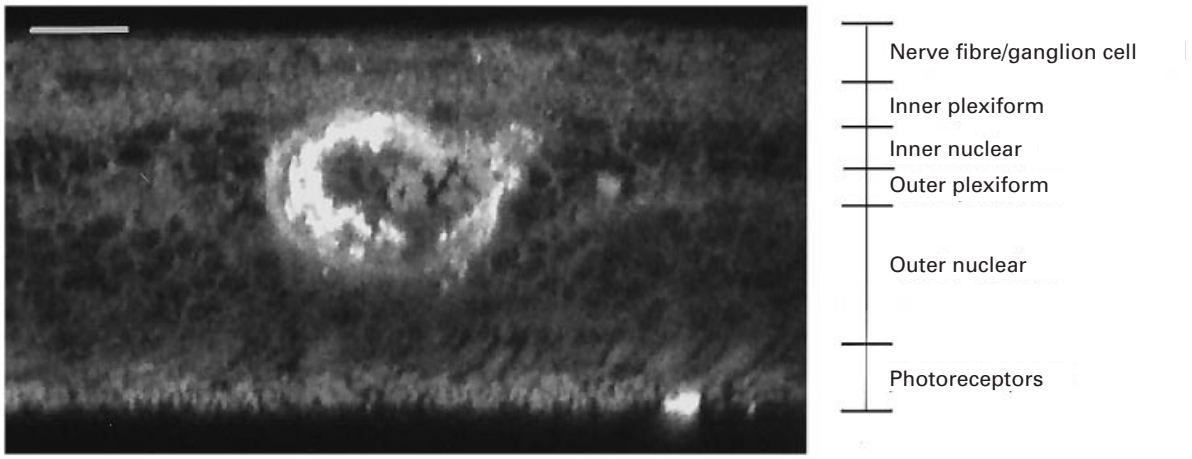

Fig. 4. xz section through the microaneurysm illustrated in Figure 3, taken with the ×60 objective lens, demonstrating the depth of the neuroretina, its various layers and the position of the microaneurysm within them. The microaneurysm originates in the inner nuclear layer (INL) and extends between the middle of the outer nuclear layer (ONL) and the INL/IPL border. Bar, 25 μm.

Microaneurysm width, i.e. the distance between the outer borders of microaneurysms when measured perpendicular to the long axis of the associated vessel, was determined from low power analysis of the same sample areas described above and ranged between 14 and 136 μm with an overall mean of 33.6 μm (Fig. 2). When microaneurysm width was compared between the 4 retinas, it was found to be smaller in retina I (comparisons with II, III and IV gave $P = 0.0021$, 0.0018 and 0.004 respectively); microaneurysm width thus varies between donors. However, when comparing microaneurysm width across the different sample areas within each retina (Fig. 2), there appeared to be no spatial variation in width in the retinal plane (xy). In support, widths of microaneurysms compared between macular and non-macular regions showed no significant difference ($P = 0.81$).

In order to establish whether there is a relationship between size and number of microaneurysms, the mean microaneurysm width was tested for correlation against counts for each sample area; no correlation was shown ($P = 0.3$).

High power analysis

In order to study individual microaneurysms in greater detail a number of randomly selected lesions were imaged and analysed at high power. This allowed information to be obtained concerning (1) microaneurysm shape, size and orientation, (2) staining characteristics, (3) the number of vessels associated with each microaneurysm and (4) the origin of microaneurysms within the many layers of the neuroretina.

Of a total of 72 randomly sampled microaneurysms the majority, 42, were 'saccular', 23 were 'focal bulges' and a minority, only 7, were 'fusiform' (Table 3). Comparison of the size (z extent) of saccular and fusiform microaneurysms (data not shown) showed no significant difference ($P = 0.32$).

The saccular microaneurysms were analysed further to determine the direction in which the outpouchings were most frequently observed. The analysis allowed 5 directions of orientation to be defined but following a χ^2 test ($P = 0.19$) there appeared to be no preferred tendency for orientation of the saccular microaneurysms.

Staining of the wall of a microaneurysm typically appeared much more intense than that of the associated vessels and in some cases saccular microaneurysms exhibited layers of staining of even greater intensity where the vessel wall bulged more prominently (Figs 3, 4). Fusiform microaneurysms and focal bulges of the vessel wall did not exhibit this asymmetric layered staining (Figs 5–8). The saccular microaneurysms were a heterogeneous population and included (1) large microaneurysms filled with erythrocytes and with either an uneven granular staining pattern of the wall (Fig. 9*a*) or the layered pattern described above (Fig. 9*b*), (2) microaneurysms with a very thin layer of staining in their walls (Fig. 9*c*), (3) microaneurysms with crenulated (or 'pitted') staining of the wall (Fig. 9*d*) and (4) occasionally microaneurysms with a very even pattern of staining (Fig. 9*d*).

At high magnification it was possible to count the number of vessels associated with each microaneurysm which varied between 1 and 5 (Table 4; Fig. 8). An association with 2 vessels was most commonly seen in all 4 retinas. In order to establish whether there

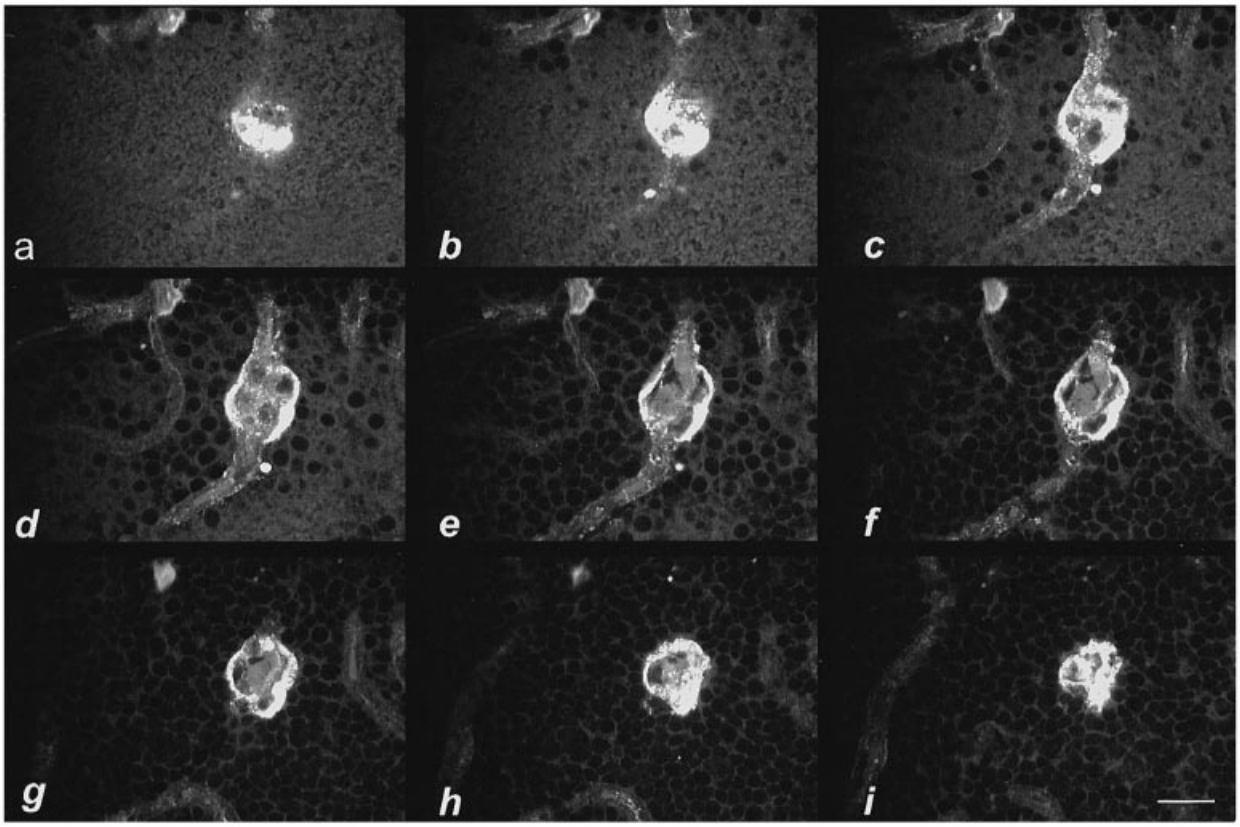

Fig. 5. Montage of images from a confocal z series captured through a fusiform microaneurysm stained for von Willebrand factor; each optical section is separated by 1.5 μm. Images were captured, using the ×60 objective lens, from the outer edge of the microaneurysm (*a*) to the inner edge of the microaneurysm (*i*). Staining of the microaneurysm wall appears evenly distributed, although much more intense than that of its associated vessels. Nuclei of the surrounding extravascular tissue are visible. Bar, 25 μm.

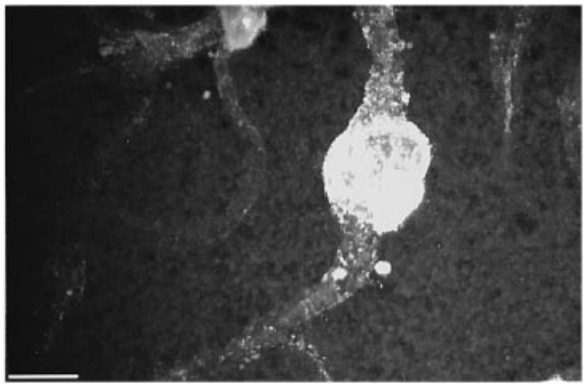

Fig. 6. Confocal maximum projection image of the z series of images illustrated in Figure 5. Nine images, each separated by 1.5 μm, were projected onto one another. The microaneurysm is fusiform and associated with only 2 vessels. Bar, 25 μm.

is a relationship between microaneurysm size and the number of associated vessels, for microaneurysms analysed at high power the z extents were tested for correlation against number of associated vessels. Highly significant negative correlation was shown ($P = 0.0064$) indicating that the larger the microaneurysm, the fewer vessels were associated with it.

Our technique allowed clear depiction of the many layers of the neuroretina in the xz images (Figs 4, 10). Microaneurysms were observed originating from the interface between the outer nuclear and outer plexiform layers to the superficial nerve fibre/ganglion cell layer (Table 5). Of the 72 microaneurysms analysed previously at high power, their origin could be identified in 70; the majority (46) originated in the INL with a further 10 originating at its borders. Furthermore, retinas II and IV showed a significantly greater probability of microaneurysms originating in the INL compared to all other layers (see statistical methods).

In order to establish whether there was a relationship between microaneurysm size and distance of microaneurysm origin from the vitreoretinal interface (VRI), for microaneurysms analysed at high power the z extents were tested for correlation against the distance (measured in number of retinal layers) of microaneurysm origin from the VRI. Highly significant positive correlation was shown ($P < 0.001$) suggesting that the larger the microaneurysm the further it originates from the VRI.

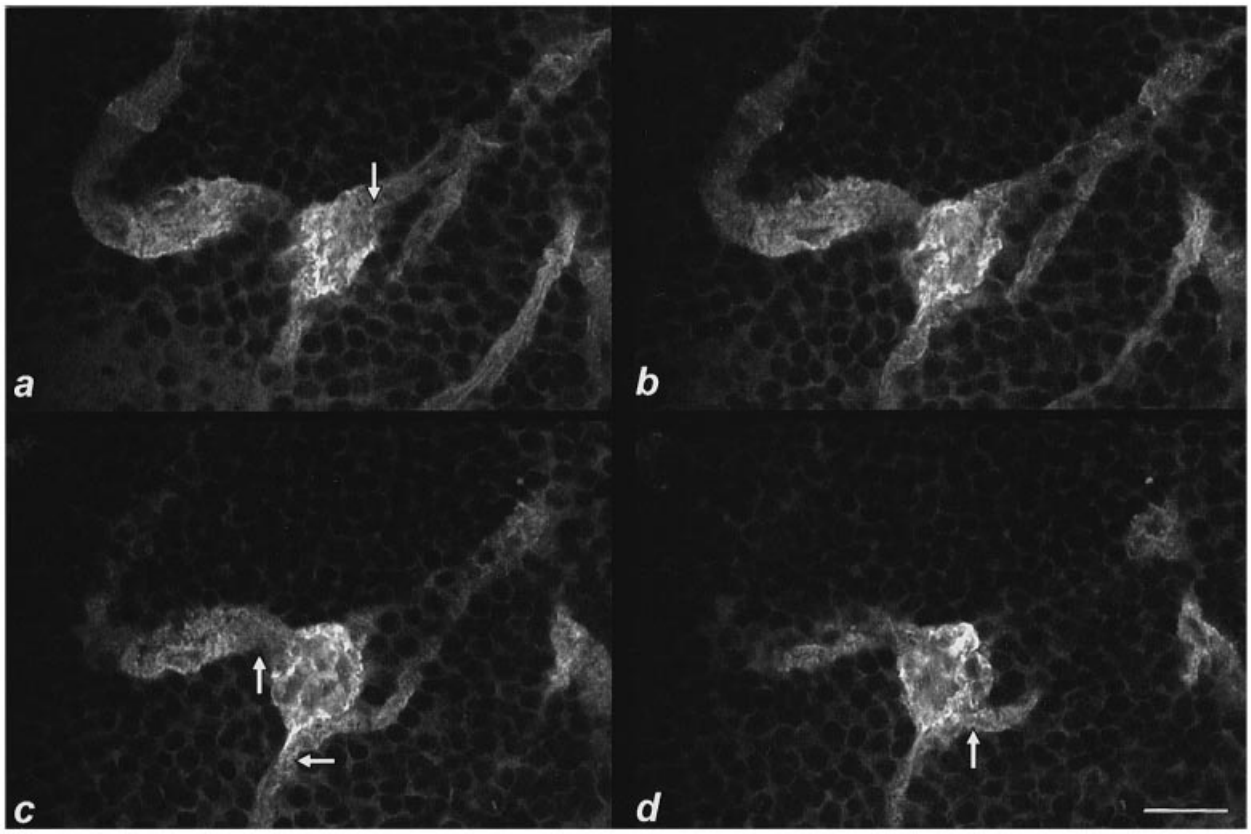

Fig. 7. Montage of images from a confocal z series captured through a focal bulge of the vessel wall stained for von Willebrand factor; each optical section is separated by 1.5 μm. Images were captured, using the ×60 objective lens, from the outer edge of the microaneurysm (*a*) to the inner edge of the microaneurysm (*d*). Arrows indicate its points of association with 4 different vessels. Bar, 25 μm.

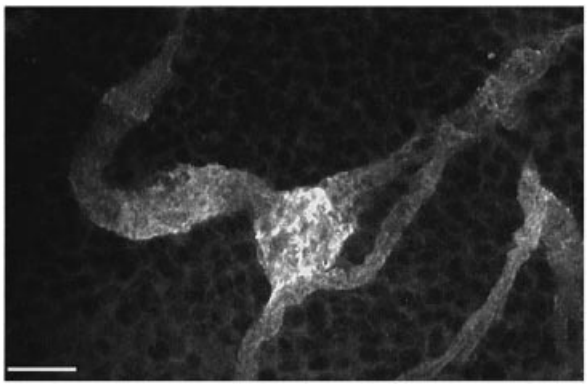

Fig. 8. Confocal maximum projection image of the z series of images illustrated in Figure 7. Four images, each separated by 1.5 μm, were projected onto one another. The microaneurysm is a focal bulge of the vessel wall and associated with 4 vessels. Bar, 25 μm.

DISCUSSION

Although microaneurysms are described in a number of other systemic and ocular disorders, they appear with greatest frequency in diabetic retinopathy (Ashton, 1951). This frequency has been shown to be an important indicator of the progression of diabetic retinopathy (Klein et al. 1989). It has previously been reported that microaneurysms are not uniformly distributed across the diabetic retina, being more prevalent in the superior temporal quadrant than the inferior nasal quadrant (Kern & Engerman, 1995) and being more numerous in the central retina (Stitt et al. 1995). Our study, which was confined to the central retina and temporal quadrant, demonstrated a random microaneurysm distribution within this region in 3 out of the 4 retinas. Furthermore, the retina which did show nonrandom distribution of microaneurysms still showed a comparable number in the macular and nonmacular areas, suggesting no preferential tendency for microaneurysm formation to occur within the visually significant macular area. The majority of microaneurysms were associated with just 2 vessels, suggesting no tendency to develop at vascular junctions.

Diabetic retinal microaneurysms ranging in size from 15 to 55 μm have been illustrated using vascular casting (Fryzkowski et al. 1991) and up to 69 μm in a trypsin digest preparation (Stitt et a1. 1995). In this study, we have demonstrated microaneurysms ranging in size between 14 and 136 μm. Although there

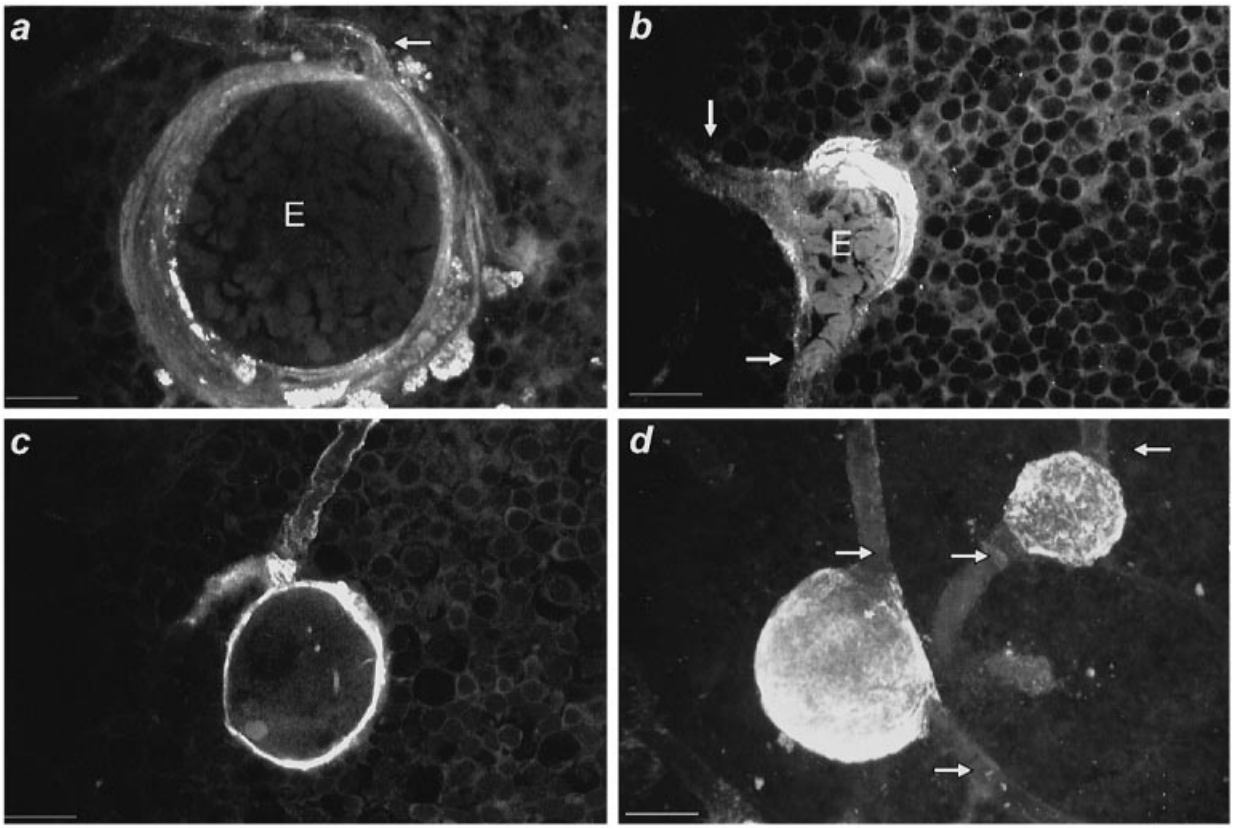

Fig. 9. (*a*) Confocal maximum projection image of 2 optical sections, separated by 3 μm, through the middle of a large saccular microaneurysm stained for von Willebrand factor, taken with the ×60 objective lens. The image shows a vessel joining the lesion (arrow). The microaneurysm is filled with erythrocytes (E) and shows both a granular and layered staining pattern of its wall. Staining appears unevenly distributed around the microaneurysm wall. Bar, 25 μm. (*b*) A single confocal image captured through the middle of a saccular microaneurysm stained for von Willebrand factor, using the ×60 objective lens. The microaneurysm is packed with erythrocytes (E). Staining of the microaneurysm wall appears more intense than that of its associated vessels (arrows) and staining is more pronounced at one side. Nuclei of the surrounding extravascular tissue are visible. Bar, 25 μm. (*c*) A single confocal image captured through the middle of a saccular microaneurysm stained for von Willebrand factor, taken with the ×60 objective lens. The microaneurysm shows a very thin layer of staining in its wall. Bar, 25 μm. (*d*) Confocal maximum projection image of 2 microaneurysms stained for von Willebrand factor. 30 images separated by 1.5 μm were captured through the lesions using the ×60 objective lens to complete a z series and used to create the single maximum projection image. The smaller microaneurysm (upper right) appears pitted, whereas the larger microaneurysm (lower left) shows an even pattern of staining. Both lesions are more intensely stained than their associated vessels (arrows). Bar, 25 μm.

Table 4. *Number of microaneurysms by vessel association and shape category**

	Retina I			Retina II			Retina III			Retina IV			
	S	F	FB	S	F	FB	S	F	FB	S	F	FB	Totals
1 vessel	0	0	0	1	0	0	0	0	0	0	0	0	1
2 vessels	6	0	6	14	0	1	9	3	3	3	1	1	47
3 vessels	1	0	5	2	0	2	3	0	2	2	1	0	18
4 vessels	0	0	1	0	0	0	0	1	0	1	0	2	5
5 vessels	0	0	0	0	0	0	0	0	0	0	1	0	1

* Analysed following random sampling of 4 retinas at high power. S, saccular; F, fusiform; FB, focal bulge. The number of vessels associated with each microaneurysm was established by examination of the images in each z series. Microaneurysms found at the tip of a cul-de-sac were classified as being associated with a single vessel.

appeared to be no spatial variation of size in the retinal plane, we have shown that differences in average microaneurysm size occur between donors and that large microaneurysms tend to occupy the deeper strata of the inner retina. Our study also allowed information to be obtained concerning mor-

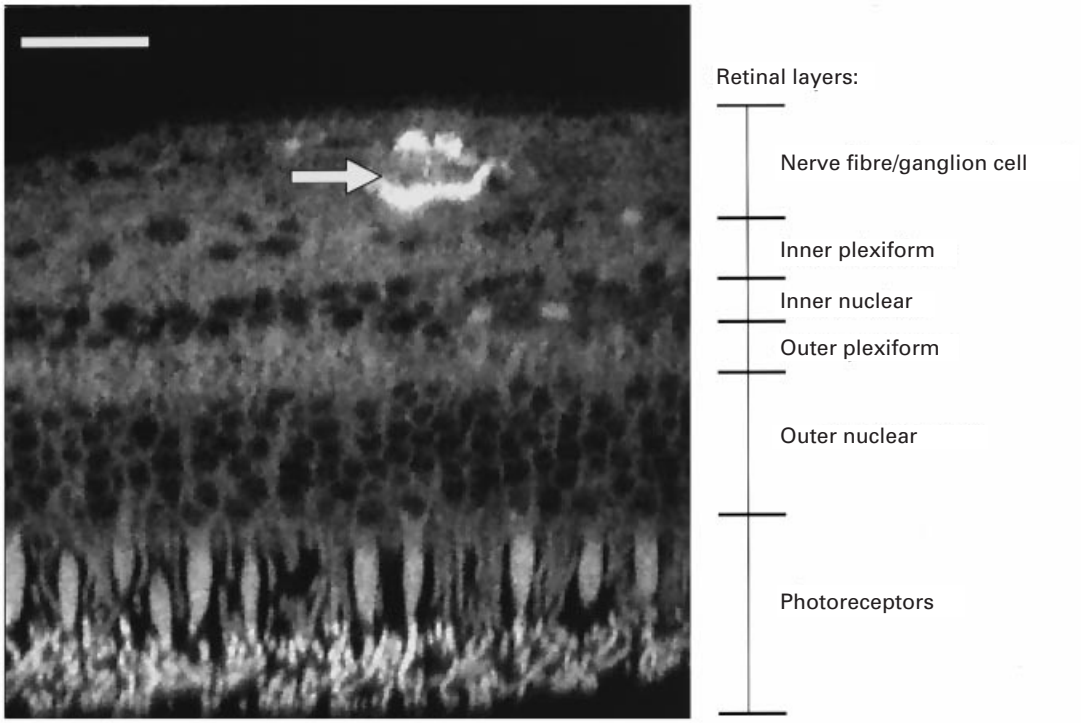

Fig. 10. xz section through the entire depth of the neuroretina taken with the ×60 objective lens. Various layers are clearly depicted and a microaneurysm (arrow) stained for von Willebrand factor is situated in the nerve fibre/ganglion cell layers. Bar, 25 μm.

Table 5. *Number of microaneurysms by origin category**

	Retina I	Retina II	Retina III	Retina IV	totals
NFL/GCL	3 (16%)	0	2 (10%)	1 (9.1%)	6 (8.6%)
Border	2 (11%)	0	0	0	2 (2.9%)
IPL	1 (5.3%)	0	0	0	1 (1.4%)
Border	3 (16%)	0	1 (5%)	0	4 (5.7%)
INL	9 (47%)	15 (75%)	12 (60%)	10 (91%)	46 (66%)
Border	0	1 (5%)	5 (25%)	0	6 (8.6%)
OPL	1 (5.3%)	3 (15%)	0	0	4 (5.7%)
Border	0	1 (5%)	0	0	1 (1.4%)

* Analysed following random sampling of 4 retinas at high power. The origin of each microaneurysm analysed within the neuroretina was identified. For every retina, the number of microaneurysms observed to originate from each layer was counted.

phology and position of microaneurysms within the depth of the retina. Previously microaneurysms have been observed mostly in the INL and occasionally the OPL on examination of transverse retinal sections using transmission electron microscopy (Stitt et al. 1995). Our method allowed us to define accurately the retinal layer in which any particular microaneurysm *originated*, as opposed to the layer(s) which it occupied. This may be important when considering the mechanism of microaneurysm formation. Our results showed that the majority of microaneurysms originated in the INL, although they were also found to originate throughout the thickness of the retina from the border of the ONL and OPL to the NFL/GCL. The occasional appearance of microaneurysms deeper than the INL is interesting and may reflect the extent of the vascular deviation from normal architecture.

The fact that the majority of microaneurysms originate in the INL and therefore in the deeper part of the inner retinal capillary plexus, may have implications when examining retinopathy using fluorescein angiography. Where the retina is thicker, i.e. at the macula, deeper fluorescence becomes 'fogged' which may therefore lead to an underestimation of the number of microaneurysms using this method and

may also obscure the relationship between microaneurysms and capillary nonperfusion (Weinhaus et al. 1995).

It has been suggested that microaneurysms are attempts at neovascularisation (Wise, 1957). The tendency of microaneurysms to originate in the INL, i.e. in the deeper capillary plexus, may implicate them in a hypoxic response. If microaneurysms are a response to hypoxia or pseudohypoxia in the outer retina we may expect them to be oriented towards that signal. However we found that microaneurysms did not appear to be oriented preferentially in any particular direction.

It is thought that microaneurysms are dynamic structures which appear and then disappear over a period of time (Kohner & Dollery, 1970; Hellstedt & Immonen, 1996). Stitt et al. (1995) described 4 ultrastructural types of microaneurysm although only 1 of these types showed an endothelium; the remainder were presumably 'late' in their development. As we immunostained for von Willebrand factor, our study only revealed microaneurysms with a surviving endothelium. We defined 3 microaneurysm morphologies (saccular, fusiform, focal bulges), which might have been thought initially to represent different stages in the development of a microaneurysm. However, as there was no difference in size between the saccular and fusiform type, it would suggest they develop independently and are not different stages in the progression of microaneurysm morphology. The staining pattern of microaneurysms was not similar throughout their population. Intense staining in saccular and fusiform microaneurysms may be indicative of a dysfunctional endothelium (Skrha, 1998) correlating with dye leakage seen clinically with fluorescein angiography.

In order to understand more fully the nature and mechanism of formation of this heterogeneous population of microaneurysms and to examine the role that reported basement membrane changes have in their development, it may be possible to extend the technique by dual staining and imaging of both endothelial cells and basement membrane components. This may also aid our understanding of the relationship of microaneurysms to focal areas of capillary nonperfusion.

ACKNOWLEDGEMENTS

The authors are grateful to Dr W. G. Bardsley for statistical assistance. This work was supported by the Guide Dogs for the Blind Association.

REFERENCES

ASHTON N (1951) Retinal microaneurysms in the non-diabetic subject. *British Journal of Ophthalmology* **35**, 189–212.

ASHTON N (1963) Studies of the retinal capillaries in relation to diabetic and other retinopathies. *British Journal of Ophthalmology* **47**, 521–538.

BARDSLEY WG (1993) SIMFIT. A computer package for simulation, curve fitting and statistical analysis using life science models. In *Modern Trends in Biothermokinetics* (ed. Schutser S, Rogoulet M, Ouhabi R, Mazat JP), pp. 455–458. New York: Plenum.

FOREMAN DM, BAGLEY S, MOORE J, IRELAND GW, MCLEOD D, BOULTON ME (1996) Three dimensional analysis of the retinal vasculature using immunofluorescent staining and confocal laser scanning microscopy. *British Journal of Ophthalmology* **80**, 246–251.

FRYCZKOWSKI AJ, CHAMBERS RB, CRAIG EJ, WALKER J, DAVIDORF FH (1991) Scanning electron microscopic study of microaneurysms in the diabetic retina. *Annals of Ophthalmology* **23**, 130–136.

HELLSTEDT T, IMMONEN I (1996) Disappearance and formation rates of microaneurysms in early diabetic retinopathy. *British Journal of Ophthalmology* **80**, 135–139.

KERN TS, ENGERMAN RL (1995) Vascular lesions in diabetes are distributed non-uniformly within the retina. *Experimental Eye Research* **60**, 545–549.

KLEIN R, MEUER SM, MOSS SE, KLEIN BE (1989) The relationship of retinal microaneurysm counts to the four year progression of diabetic retinopathy. *Archives of Ophthalmology* **107**, 1780–1785.

KOHNER EM, Dollery CT (1970) The rate of formation and disappearance of microaneurysms in diabetic retinopathy. *European Journal of Clinical Investigation* **1**, 167–171.

RODRIQUEZ J, DEINHARDT F (1960) Preparation of a semipermanent mounting medium for fluorescent antibody studies. *Virology* **12**, 316–317.

SHOTTON D, WHITE, N (1989) Confocal scanning microscopy: three-dimensional biological imaging. *Trends in Biological Science* **14**, 435–439.

SKRHA, J (1998) Possible markers of diabetic vascular disease. *Diabetes Reviews International* **7**, 12–14.

STITT AW, GARDINER TA, ARCHER DB (1995) Histological and ultrastructural investigation of retinal microaneurysm development in diabetic patients. *British Journal of Ophthalmology* **79**, 362–367.

WEINHAUS RS, BURKE JM, DELORI FC, SNODDERLY DM (1995) Comparison of fluorescein angiography with microvascular anatomy of Macaque retinas. *Experimental Eye Research* **61**, 1–16.

WISE GN (1957) Retinal microaneurysms. *Archives of Ophthalmology* **57**, 151–156.